Nucleic Acids Research, 2023, **51**, 11652–11667
https://doi.org/10.1093/nar/gkad919
Advance access publication date: 27 October 2023
Gene regulation, Chromatin and Epigenetics

LSM14B is essential for oocyte meiotic maturation by regulating maternal mRNA storage and clearance

Yanling Wan[1,2,3,4,†], Shuang Yang[5,†], Tongtong Li[1,2,3,4], Yuling Cai[1,2,3,4], Xinyue Wu[1,2,3,4], Mingyu Zhang[1,2,3,4], Tahir Muhammad[1,2,3,4,6,7], Tao Huang[1,2,3,4,8], Yue Lv[8,9], Wai-Yee Chan[1,2,4,8], Gang Lu[1,2,4,8], Jingxin Li[5], Qian-Qian Sha[10,*], Zi-Jiang Chen[1,9,2,3,4,8,11,12,*] and Hongbin Liu[1,2,3,4,8,11,*]

[1]Center for Reproductive Medicine, Shandong University, Jinan, Shandong 250012, China
[2]Key Laboratory of Reproductive Endocrinology of Ministry of Education, Shandong University, Jinan, Shandong 250012, China
[3]Shandong Provincial Clinical Medicine Research Center for Reproductive Health, Jinan, Shandong 250012, China
[4]State Key Laboratory of Reproductive Medicine and Offspring Health, Jinan, Shandong 250012, China
[5]Department of Physiology School of Basic Medical Sciences, Cheeloo College of Medicine, Shandong University, Jinan, Shandong 250012, China
[6]Department of Cell Biology and Anatomy, NY Medical College, 15 Dana Road, Valhalla, NY 10595, USA
[7]Institute of Molecular Biology and Biotechnology, The University of Lahore, Lahore 54000, Pakistan
[8]CUHK-SDU Joint Laboratory on Reproductive Genetics, School of Biomedical Sciences, the Chinese University of Hong Kong, Hong Kong 999077, China
[9]Shandong Key Laboratory of Reproductive Medicine, Shandong Provincial Hospital Affiliated to Shandong First Medical University, Jinan, Shandong 250012, China
[10]Fertility Preservation Laboratory, Reproductive Medicine Center, Guangdong Second Provincial General Hospital, Guangzhou, Guangdong 510317, China
[11]Research Unit of Gametogenesis and Health of ART-Offspring, Chinese Academy of Medical Sciences, Jinan, Shandong 250012, China
[12]Shanghai Key Laboratory for Assisted Reproduction and Reproductive Genetics, Shanghai 200135, China

[*]To whom correspondence should be addressed. Tel: +86 531 85651190; Fax: +86 53187068226; Email: hongbin_sduivf@aliyun.com
Correspondence may also be addressed to Zi-Jiang Chen. Email: chenzijiang@hotmail.com
Correspondence may also be addressed to Qian-Qian Sha. Email: shaqianqian@zju.edu.cn
[†]The authors wish it to be known that, in their opinion, the first two authors should be regarded as Joint First Authors.
Present address: Yanling Wan, Department of Obstetrics and Gynecology, Peking University People's Hospital, Beijing 100034, China.

Abstract

Fully grown oocytes remain transcriptionally quiescent, yet many maternal mRNAs are synthesized and retained in growing oocytes. We now know that maternal mRNAs are stored in a structure called the mitochondria-associated ribonucleoprotein domain (MARDO). However, the components and functions of MARDO remain elusive. Here, we found that LSM14B knockout prevents the proper storage and timely clearance of mRNAs (including Cyclin B1, Btg4 and other mRNAs that are translationally activated during meiotic maturation), specifically by disrupting MARDO assembly during oocyte growth and meiotic maturation. With decreased levels of storage and clearance, the LSM14B knockout oocytes failed to enter meiosis II, ultimately resulting in female infertility. Our results demonstrate the function of LSM14B in MARDO assembly, and couple the MARDO with mRNA clearance and oocyte meiotic maturation.

Received: May 5, 2023. **Revised:** October 1, 2023. **Editorial Decision:** October 3, 2023. **Accepted:** October 9, 2023

Graphical abstract

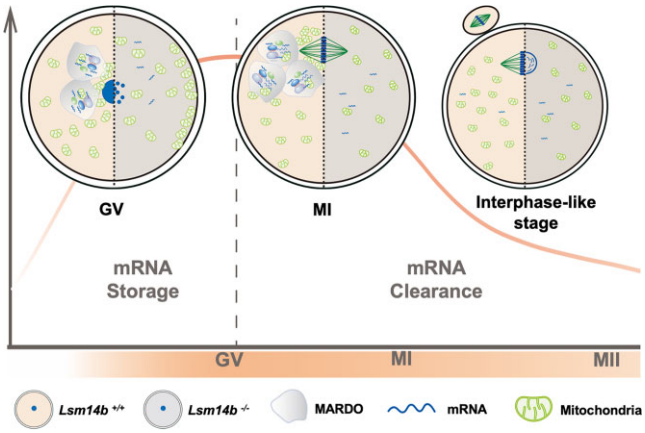

Introduction

Proper storage and efficient clearance of maternal mRNAs are essential for mammalian oocyte growth, meiotic maturation and subsequent early embryonic development (1,2). Numerous mRNAs are synthesized and accumulated in growing oocytes and these remain relatively stable until they are fully grown (3–5). Fully grown germinal vesicle (GV) oocytes display two distinct chromatin morphologies, categorized as surrounded nucleolus (SN) or non-surrounded nucleolus (NSN) oocytes (6). SN oocytes exhibit global transcriptional quiescent, while NSN oocytes maintain transcriptional activity before resumption of oocyte meiosis (7). SN oocytes with accumulation of those transcripts required for meiotic maturation and early embryogenesis have higher developmental potential compared with NSN oocytes (8). The process of oocyte meiotic maturation and early embryogenesis is mainly regulated by protein synthesis from pre-stored maternal mRNAs that are transcribed and accumulated during oocyte growth (9).

Oocyte meiotic maturation begins with meiotic resumption via GV breakdown (GVBD) (6). The resumption of meiosis triggers a transition from mRNA stability to instability (3,10,11). Then massive but target-specific and temporally selective clearance of transcripts occurs controlled by cytoplasmic deadenylation, which is facilitated by maternal factors (e.g. BTG4, PABPN1L, CNOT6L and CNOT7); this process of mRNA clearance is referred to as maternal decay (M-decay) (3,12). M-decay in meiotic maturation is a prerequisite for the developmental potential of oocytes (1). BTG4 (B-cell translocation gene 4) is one such maternal factor; it is expressed exclusively in oocytes and early embryos, and has been shown to facilitate the clearance of maternal mRNAs (4). Through bridges between CCR4–NOT transcription complex subunit 7 (CNOT7) and eukaryotic translation initiation factor 4E (EIF4E), BTG4 mediates maternal mRNA degradation by shortening the poly(A) tails in mouse oocytes during meiotic maturation (extremely in the meiosis I and II transition) and the maternal-to-zygotic transition (MZT) (3,10,12,13). Oocytes and embryos derived from *Btg4* knockout female mice exhibit impaired M-decay, and zygotes arrest at the one-to two-cell stage (4).

The transcripts accumulated in oocytes are stored in a dormant state, with selective activation for translation at the appropriate developmental stage and timely degradation to coordinate oocyte maturation events (5). Recent studies showed that maternal mRNAs are stored in a structure called a mitochondria-associated ribonucleoprotein domain ('MARDO') which functions as a storage site for pre-existing mRNAs in oocytes of various mammalian species (14). MARDO is first evident in NSN oocytes, becoming most prominent in metaphase I (MI) oocytes, and dispersing as oocytes transition from meiosis I to meiosis II (14).

During oocyte meiotic maturation, oocytes enter meiosis II without going through interphase (15–17). To enter meiosis II, the reactivation of maturation-promoting factor (MPF) is required; this complex comprises cyclin-dependent kinase1 (CDK1) and its regulatory subunit Cyclin B1 (14,18). The activity of MPF is determined in large part by the increased level of Cyclin B1, while Cyclin B1 is degenerated by the anaphase-promoting complex/cyclosome (APC/C) (19–21). Considering the translational silence of GV oocytes, abundant storage of *Cyclin B1* mRNA in GV oocytes is required for the restoration of Cyclin B1 during the meiosis I to II transition (22).

LSM14 (also named RAP55) is a 55 kDa RNA-binding protein that is evolutionarily conserved across vertebrate species (23), most of which have two paralogous proteins: LSM14A and LSM14B (24,25). Studies in HeLa cells showed that LSM14 is present in P-bodies (which function in storing mRNAs) (26). In mitosis, LSM14 has been reported to regulate the mitotic G_2/M transition (24,27). A previous study reported that knockdown of LSM14A in oocytes had no effect on oocyte maturation, whereas knockdown of LSM14B resulted in MI arrest (28). However, the physiological function(s) of LSM14B remain unknown.

Here, fertility testing showed that female *Lsm14b* knockout mice are infertile, and a subsequent detailed analysis ascribed the reproductive defect to the chromatin morphologies in GV oocytes and the meiosis I and II transition of oocyte meiotic maturation. RNA-seq revealed a reduction in the extent of mRNA storage in GV oocytes, as well as aberrant mRNA clearance during meiotic maturation of *Lsm14b* knockout oocytes. Upon integrating transcriptomics and proteomics datasets, we identified a decrease in the storage of *Btg4* and *Cyclin B1* mRNA in GV oocytes, as well as impaired translation in oocytes obtained 14 h after human chorionic gonadotrophin (hCG) injection (denoted as 'interphase-like oocytes') from *Lsm14b* knockout mice. Using microinjection, we provide evidence that LSM14B promotes MARDO assembly during meiosis I. Thus, our study reveals that LSM14B regulates mRNA storage in GV oocytes and M-decay during oocyte meiotic maturation, and promotes MARDO assembly;

disrupting LSM14B function blocks the meiosis I to II transition, ultimately resulting in female infertility.

Materials and methods

Animals

All mice were maintained in a specific pathogen-free environment, and all animal experiments were conducted in accordance with the guidelines and regulations of Shandong University. The experimental protocol was approved by the Animal Care and Research Committee of Shandong University. *Lsm14b* knockout mice were generated through CRISPR/Cas9 [clustered regularly interspaced palindromic repeats (CRISPR)/CRISPR-associated protein 9]-mediated genome engineering in a C57BL/6J background by GemPharmatech Co. Ltd. A total of 695 bp of the *Lsm14b* gene were removed, which caused complete removal of exons 3–7. F_0 founder animals were identified by polymerase chain reaction (PCR) followed by sequence analysis, and were subsequently bred with wild-type (WT) mice to assess germline transmission and to generate F_1 animals.

Collection of ocytes and embryos

For collection of GV oocytes, mice were humanely euthanized and ovaries were dissected from 3-week-old female mice 46 h after injection with 5 IU of pregnant mare serum gonadotrophin (PMSG). The ovaries were transferred to M2 medium (Sigma-Aldrich) and punctured with a 7-gauge needle to release cumulus–oocyte complexes (COCs), then the cumulus cells were gently removed from the COCs by a narrow-bore glass pipette.

For the collection of MI and MII oocytes, 6-week-old female mice were injected with 5 IU of hCG after 46 h of PMSG injection and then MI-stage oocytes were collected after 8 h of hCG injection, while MII-stage oocytes were collected according to specific experimental needs. COCs were harvested from the oviducts and digested with hyaluronidase (300 IU/ml). To obtain early embryos, superovulated female mice were mated with 12-week-old WT males for an entire night. Vaginal plugs were checked the following morning, and mice with plugs were considered to be 0.5 days post-coitum (dpc). Zygotes, two-cell, four-cell, eight-cell, morula embryos and blastocysts were collected at 1, 1.5, 2, 2.5, 3.5 and 4–4.5 dpc, respectively.

mRNA preparation and microinjection

To prepare mRNA for microinjection, the plasmid was linearized with a restriction enzyme and then served as a template for *in vitro* transcription using the mMESSAGE mMACHINE T7 Ultra kit (Thermo Fisher Scientific, AM1345). Poly(A) tails (~200–250 bp) were added to the transcribed mRNAs using the mMESSAGE mMACHINE® T7 Ultra kit. Synthesized mRNA was purified by LiCl precipitation then dissolved in nuclease-free water and quantified using a NanoDrop spectrophotometer (Thermo Fisher Scientific, ND-LITE), and stored at −80°C.

All microinjections were performed using an ECLIPSE Ti2 inverted microscope (Nikon, ECLIPSE Ti2). GV oocytes were incubated in M2 medium containing 2.5 μM milrinone to inhibit spontaneous GVBD for later microinjection. Approximately 10 pl of mRNAs at a concentration of 500 ng/μl were microinjected into each oocyte. After microinjection, oocytes were cultured in M16 medium containing 2.5 μM milrinone for 12 h at 37°C and 5% CO_2 to ensure full translation of mRNA followed by a thorough wash, and cultured in fresh M16 medium. (We constructed the plasmid of LSM14B, while ZAR1 was a generous gift from Dr Qianqian Sha.)

Western blotting

For immunoblot experiments, 100 oocytes were collected and quickly washed three times with phosphate-buffered saline (PBS), then lysed in 2× loading buffer (containing protease inhibitor). The samples were heated for 5 min at 95°C before being resolved on a 12-well FuturePAGE 12% protein gel of 1.5 mm thickness (ACE Biotechnology, ET12012Gel) with 4-morpholinepropane sulfonic acid (MOPS)–sodium dodecylsulfate (SDS) running buffer (ACE Biotechnology, F00004Gel). Then proteins were transferred onto a 0.45 μm polyvinylidene fluoride membrane (Sigma Aldrich, IEVH00005) and the membranes were blocked in Tris-buffered saline–Tween (TBST) containing 5% skimmed milk for 1 h at room temperature and then incubated with the indicated primary antibodies overnight at 4°C. Primary antibodies against LSM14B (1/1000 dilution; Novus Biologicals, NBP2-76362), ZAR1 (1/1000 dilution; a generous gift from D. Hengyu Fan), EIF4E1B and EIF4ENIF1 (1/1000 dilution; generous gifts from Dr Youqiang Su), DDX6 (1/1000 dilution; Proteintech, 14632–1-AP), Cyclin B1 (1/1000 dilution; CST, 4138T), glyceraldehyde phosphate dehydrogenase (GAPDH; 1/1000 dilution; Proteintech, 60004–1-Ig) and β-actin (1/1000 dilution; Proteintech, 66009–1-Ig) were used in this study. After washing three times with TBST, the membranes were incubated with the appropriate horseradish peroxidase (HRP)-conjugated secondary antibody for 1.5 h at room temperature. Secondary antibodies used were HRP-conjugated goat anti-rabbit (ZSGB-BIO, ZB-2301), anti-mouse (Dako, catalog no. P0260) and anti-mouse (ZSGB-BIO, ZB-2305). All secondary antibodies were diluted 1:2000 for use. Finally, the membranes were detected by the enhanced chemiluminescence detection system (BIO-RAD, ChemiDoc MP Imaging System).

RNA extraction and RT–PCR validation

A REPLI-g WTA Single Cell Kit (QIAGEN, 150063) was used for extraction of total RNA of oocytes, and cDNA was acquired ultimately according to the manufacturer's protocols. cDNA was stored at –80°C and diluted with RNase-free water at 1:100 for use. An RNeasy Plus Micro Kit (QIAGEN, 74034) was used for extraction of total RNA of tissues. Genomic DNA (gDNA) was eliminated by digesting with genomic DNA eraser buffer, and cDNA was obtained by reverse transcription of RNA using the PrimeScript RT reagent Kit with gDNA Eraser (Takara, RR047A). To measure the values of gene-specific primers, the reverse transcription—PCR (RT–PCR) was performed in triplicate. Relative mRNA levels were normalized to the level of endogenous β-actin mRNA (internal control). The relative transcription levels of the samples were compared with those of the control, followed by subsequent determination of the fold change (FC). Finally, the relative expression levels of targeted genes were calculated using the $2^{-\Delta\Delta CT}$ method. The sequences of the genotyping primers are listed in Supplementary Table S1.

Histological analysis

Ovaries were collected and fixed in 4% PBS-buffered formalin overnight. After dehydration, the ovaries were embedded in paraffin, serially sectioned at 5 mm thickness and stained with hematoxylin. The slides were imaged under a microscope equipped with a camera (OLYMPUS, BX53F2).

Immunofluorescence

Oocytes were collected and fixed in 4% PBS-buffered formalin for 30 min and then permeabilized with 0.3% Triton X-100 in PBS for 20 min at room temperature. Then, oocytes were blocked in 1% bovine serum albumin (BSA)-supplemented PBS for 1 h at room temperature followed by incubation with primary antibodies at 4°C overnight. Primary antibodies against HSP60 (1/400 dilution; Cell Signaling Technology, 12165T), FLAG (1/400 dilution; Sigma Aldrich, F3165) and α-TUBULIN-FITC (1/400 dilution; Sigma Aldrich, F2168) were used in this study. After washing three times, oocytes were incubated with appropriate secondary antibody for 1 h at room temperature before staining with 4′,6-diamidino-2-phenylindole (DAPI) for 10 min. Finally, oocytes were mounted on glass slides and imaged with a confocal microscope (Andor Technology Ltd, Belfast, UK).

Visualization of the mitochondria by MitoTracker Green

MitoTracker Green (1/2000, Invitrogen, M7514) was first diluted with M16 medium to make culture droplets and placed in an incubator at 37°C to equilibrate. Oocytes were then transferred to the droplets and incubated at 37°C for 30 min. After counterstaining with Hoechst (1/800 dilution, Thermo Fisher Scientific, R37605), oocytes were moved to a glass bottom culture dish and imaged under a laser scanning confocal microscope (Andor Technology Ltd). The distribution of mitochondria was reflected by MitoTracker Green staining. All photos for analysis were taken with the same intensity parameters and exposure time settings. The distribution of mitochondrial signals in a oocyte was evaluated objectively with a Clock Scan plugin or plot profiles plugin for ImageJ as described previously (29,30).

Determination of ATP levels

An ATP testing assay kit (Beyotime, S0026) was used to measure total ATP content of oocytes. Briefly, 50 oocytes were added to 200 μl of lysis buffer and centrifuged at 12 000 *g* for 5 min at 4°C. The supernatant was collected and mixed with testing buffer, then the ATP concentration was detected on a luminescence detector (EnSpire Multimode Plate Reader). A standard curve ranging from 0.01 to 1 mM was generated and was used to calculate the total ATP contents.

Detection of ROS generation

A reactive oxygen species (ROS) assay kit (Beyotime, S0033S) was used to detect ROS generation in oocytes. The dichlorofluorescein diacetate (DCFH-DA) probe was diluted with M16 medium to make culture droplets and they were placed in an incubator at 37°C to equilibrate for 30 min. Thereafter, oocytes were transferred to the droplets containing 10 μM DCFH-DA and incubated (in the dark) for 30 min at 37°C. Then oocytes were washed three times, moved to a glass bottom culture dish and imaged under a laser scanning confocal microscope (Andor Technology Ltd). All photos for analysis were taken with the same intensity parameters and exposure time settings. The ROS level was quantified by analyzing the fluorescence intensity of the oocytes by using ImageJ software.

mRNA-FISH

The Ribo Fluorescent in Situ Hybridization Kit (RIBOBIO,C10910) was used for RNA-fluorescence *in situ* hybridization (FISH). Oocytes derived from WT and *Lsm14b* knockout females were fixed in 4% PBS-buffered formalin for 30 min at room temperature. After extensive washing with wash buffer, oocytes were permeabilized with homemade permeabilization solution (PBS containing 1% Triton X-100) for 30 min at room temperature. They were then washed again before being treated with pre-hybridization solution (blocking solution diluted 1/100 with pre-hybridization buffer) and incubated at 37°C for 30 min. Meanwhile, the hybridization solution (blocking solution diluted 1/100 with hybridization buffer) was heated at 37°C for 30 min. Probe sets of mRNAs of interest [poly(A), *Btg4* and *CyclinB1*] were mixed and diluted 1:50 with pre-warmed probe hybridization solution and incubated at 37°C overnight in the dark. The next day, the oocytes were washed with homemade wash buffer for 10 min at 42°C in the dark. Finally, oocytes were stained with Hoechst 33342 in PBT-BSA solution (PBS containing 0.1% Triton X-100 and 3% BSA) for 30 min at room temperature to label DNA.

EU incorporation assay

A Click-iT RNA Alexa Fluor 488 Imaging Kit (Thermo Fisher Scientific, C10329) was used to detect the new RNA synthesis level of oocytes. Firstly, 5-ethynyluridine (EU) was diluted with M16 medium to make culture droplets and these were placed in an incubator at 37°C to equilibrate for 30 min. Thereafter, oocytes were transferred to the droplets containing 1 mM EU and incubated for 1 h at 37°C before fixation, permeabilization and staining with reaction buffer according to the manufacturer's protocol. After counterstaining with Hoechst 33342, oocytes were mounted on glass slides and imaged with a confocal microscope (Andor Technology Ltd).

RNA-seq and data analysis

Fifteen oocytes at each of the three stages (GV, MI and MII) were collected from WT and *Lsm14b*$^{-/-}$ mice, with three replicates per sample. After washing three times in PBS, the samples were collected in tubes with lysis component and RNase inhibitor and then transferred to a –80°C freezer with liquid nitrogen. The samples were sent on dry ice to Beijing Annoroad Gene Technology Co., Ltd, which was responsible for transcriptome sequencing and data analysis. The raw data were filtered to obtain high-quality, clean data which were subsequently mapped to a reference genome using HISAT2 v2.1.0. The SAM output from this alignment was then converted into BAM format using SAMtools version 0.1.5. HTSeq v0.6.0 was used to determine the read counts mapped to each gene. Finally, expression levels of the targeted genes were evaluated using the metric of reads per kilobase of exon transcript per million mapped reads (RPKM).

The DESeq2 package (version 1.38.3) was utilized to identify differentially expressed genes (DEGs) between the two

groups (three replicates in each group). Genes were defined as DEGs when logFC was ≥ 2 and ≤ -2, with a *P*-value cut-off of 0.05. To perform Gene Ontology (GO) and pathway enrichment analyses, clusterProfiler (version 4.0.5) and Metascape were employed. For the GO enrichment analysis of DEGs, the number of genes in each GO term was calculated according to the GO resource (http://geneontology.org/), and then a hypergeometric test was applied to find out the significantly enriched GO Terms compared with the whole genomic background. Setting calibrated *P*-value of GO term which lower than 0.05 was different gene expression significantly enriched. A hypergeometric test was applied to the enrichment analysis of each pathway in the Kyoto Encyclopedia of Genes and Genomes (KEGG) to find the pathway with significant enrichment of DEGs.

The RNA-seq data from the *Lsm14b*$^{-/-}$ mice were compared with those of the WT mice during the different developmental stages of oocytes, and the mRNA expression levels were partially verified by real-time quantitative PCR experiments. All percentages or values from at least three biological replicates were expressed as the mean ± the standard error of the mean (SEM), and statistical analysis was performed with paired *t*-tests by GraphPad Prism 9.5.1 (GraphPad Software, San Diego, CA, USA).

Proteomics data analysis

One hundred MII stage oocytes were collected from WT and *Lsm14b*$^{-/-}$ mice, with three replicates per sample. After washing three times in PBS, the samples were collected in tubes with lysis buffer and then transferred to a –80°C freezer with liquid nitrogen. The samples were sent on dry ice to Hangzhou JingJie Biotechnology Co., Ltd, who were responsible for proteomics testing and data analysis. A cut-off of the adjusted *P*-value of 0.05 (false discovery rate adjusted) along with a $\log_2$FC of 2 was applied to determine significantly regulated proteins in the WT and *Lsm14b*$^{-/-}$ comparison.

In this study, the GO annotations of proteins were categorized into three groups: Biological Process, Cellular Component and Molecular Function. To determine the significance of GO enrichment of differentially expressed proteins, Fisher's exact test was employed with identified proteins as the background, and a P-value < 0.05 was regarded as significant. The KEGG database was used for pathway enrichment analysis, and Fisher's exact test was used to evaluate the significance of KEGG pathway enrichment of differentially expressed proteins with identified proteins as the background. A P-value < 0.05 was considered significant. Furthermore, Gene Set Enrichment Analysis (GSEA) was performed to identify specific biological pathway gene sets that were significantly associated with the expression levels between two groups of samples.

Co-immunoprecipitation (Co-IP)

At 48 h after transfection, the transfected HeLa cells were quickly washed in cold PBS twice and lysed in lysis buffer (Beytime, P0013) with Protease Inhibitor Cocktail (1/25 dilution, Roche, 04693116001) at 4°C for 30 min, and then centrifuged at 12 000 *g* for 15 min to harvest the supernatant. Next, extracted total proteins were incubated with target antibodies and anti-IgG rabbit antibody overnight at 4°C. Protein A–agarose (Roche, 11134515001) and Protein G–agarose (Roche, 11243233001) were added to each sample and incubated for 1 h at room temperature. Then, a portion was taken from the sample and the target antibody was added to it, and the mixture was incubated at 37°C for 30 min. After being washed three times in lysis buffer (Beytime, P0013), the co-immunoprecipitated proteins were resuspended with loading buffer and heated for 10 min at 95°C for further western blot assays.

Statistical analysis

Data are presented as the mean ± SEM of three independent experiments/samples unless otherwise specified. Two-tailed unpaired Student's *t*-tests or the one-way analysis of variance (ANOVA) statistical tool was applied to determine the group comparison value when necessary: $^{*}P < 0.05$; $^{**}P < 0.01$, $^{***}P < 0.001$ and $^{****}P < 0.0001$. All analyses were performed using the GraphPad Prism 9.5.1 (GraphPad Software).

Results

LSM14B is highly expressed in oocytes, and *Lsm14b* knockout in mice causes female infertility

We first investigated the expression pattern of the LSM14B protein during oocyte maturation and transition into embryos. We profiled *Lsm14b* mRNA levels in diverse somatic tissues, oocytes and early embryos by qPCR. The *Lsm14b* mRNA levels were noticeably higher in oocytes than in somatic tissues (Figure 1A). We noted a trend wherein the *Lsm14b* mRNA level is highest in GV stage oocytes, lower in zygotes and extremely low or absent in two-cell embryos (Figure 1A). Additionally, immunoblotting against LSM14B showed high accumulation in GV oocytes, with the abundance decreasing during meiotic maturation and becoming marginal in two-cell embryos (Figure 1B).

To study the *in vivo* function of LSM14B, we generated a *Lsm14b* knockout mouse strain using CRISPR/Cas9, based on a 695 bp deletion from exons 3–7 (Figure 1C). qPCR and immunoblotting confirmed that the *Lsm14b* mRNA and LSM14B protein were already completely absent in GV stage oocytes (Figure 1D, E). The body and ovary size of *Lsm14b* knockout mice did not differ obviously from those of WT mice (Figure 1F). In addition, *Lsm14b* knockout female mice displayed normal ovarian histology (Figure 1G). Nevertheless, fertility testing indicated that the *Lsm14b* knockout female mice were completely infertile (Figure 1H).

Lsm14b knockout oocytes fail to enter MII

To explore the cause of infertility of *Lsm14b* knockout female mice, we looked at oocyte meiotic progression. We examined the meiosis II progression of the *Lsm14b* knockout oocytes. We collected COCs from antral follicles of WT and *Lsm14b* knockout mice by needle puncturing under a stereoscope 46 h after injection with 5 IU of PMSG, then gently removed the cumulus cells from the COCs using a narrow-bore glass pipette. A total of 16.75% of oocytes from COCs had an NSN collected from WT samples, contrasting with the 57.58% observed for the *Lsm14b* knockout samples (Figure 2C).

We also collected ovulated oocytes by injecting 6-week-old female mice with 5 IU of hCG after 46 h of PMSG injection; MII stage oocytes were collected according to specific experimental needs (oocytes ovulated 12, 14 and 16 h after hCG). COCs were harvested from the oviducts and were digested

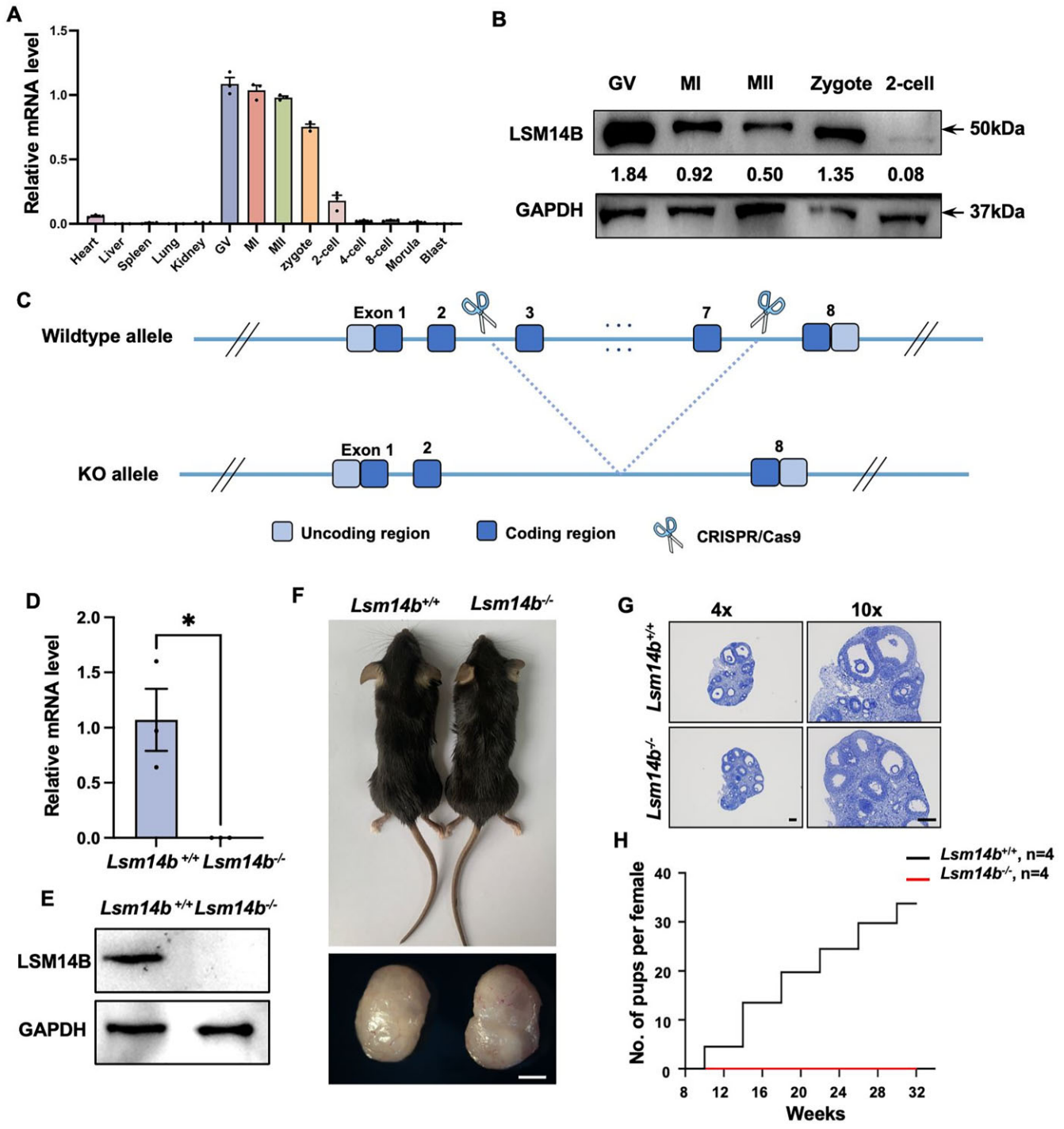

Figure 1. Profiling LSM14B expression in oocytes and early embryos, and generation of *Lsm14b* knockout mice. (**A**) qPCR results for *Lsm14b* expression in oocytes, pre-implantation embryos and somatic tissues of mice. *Gapdh* was used as an internal control. $n = 3$ biological replicates. (**B**) Immunoblotting results showing LSM14B expression levels in oocytes during meiotic maturation and embryos at the indicated developmental stages. LSM14B and GAPDH band densities were quantified, and LSM14B/GAPDH ratios were calculated. Total proteins from 100 oocytes were loaded in each lane. GAPDH was blotted as a loading control. (**C**) The *Lsm14b* knockout strategy in mice. (**D**) qPCR results for *Lsm14b* expression in GV oocytes of WT and *Lsm14b* knockout females. *Gapdh* was used as an internal control. $n = 3$ biological replicates. Error bars = SEM. $^*P < 0.05$ by two-tailed Student's *t*-tests. (**E**) Immunoblotting results showing LSM14B in GV oocytes of WT and *Lsm14b* knockout females. Total proteins from 100 oocytes were loaded in each lane. GAPDH is blotted as a loading control. (**F**) Morphology of mice and ovaries at postnatal day 56. Scale bar = 1 mm. (**G**) Hematoxylin staining of ovary sections from WT and *Lsm14b* knockout female mice. Scale bar = 200 μm. (**H**) Cumulative numbers of pups per female during the indicated time windows of the fertility test. The numbers of analyzed mice are indicated (*n*).

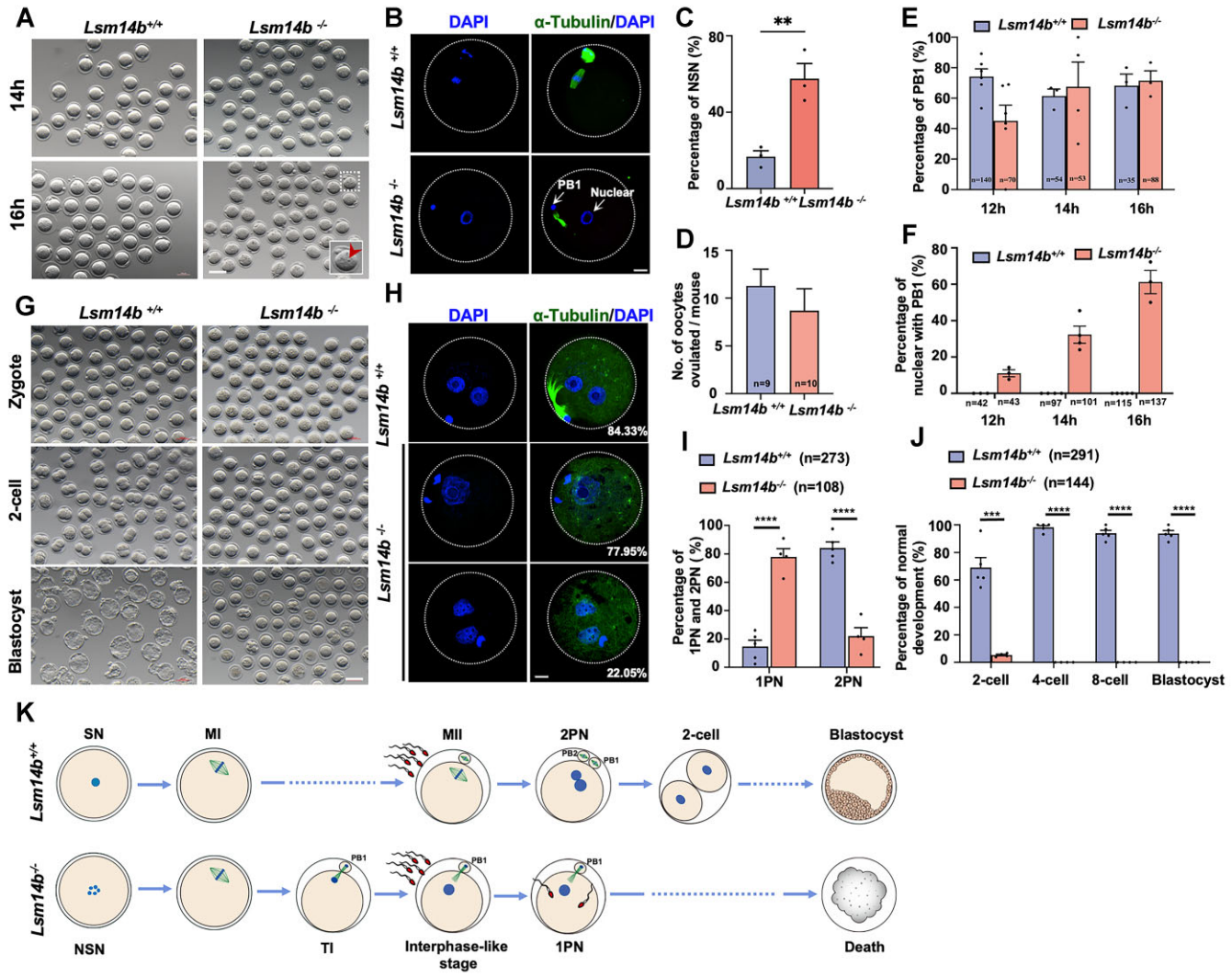

Figure 2. *Lsm14b* knockout oocytes display embryogenesis defects. (**A**) Representative images of oocytes derived from WT and *Lsm14b* knockout mice *in vivo* at 14 and 16 h after hCG injection. Scale bar = 100 μm. (**B**) Immunofluorescence analysis of oocytes collected from WT and *Lsm14b* knockout mice at 16 h after hCG injection. Scale bar = 20 μm. (**C**) The rates of SNs and NSNs collected from WT and *Lsm14b* knockout mice. Data are presented as the mean ± SEM. $^{**}P < 0.01$. (**D**) The number of oocytes ovulated from WT and *Lsm14b* knockout mice. The numbers of analyzed mice are indicated (*n*). (**E**) The percentages of oocytes with a first polar body (PB1) at 12, 14 and 16 h after ovulation induction (via hCG injection, 5 IU). The numbers of analyzed oocytes are indicated (*n*). (**F**) The percentages of oocytes with a PB1 and a nucleus at 12, 14 and 16 h after ovulation induction (via hCG injection, 5 IU). The numbers of analyzed oocytes are indicated (*n*). (**G**) Representative images of pre-implantation embryos at different stages derived from WT and *Lsm14b* knockout mice. (**H**) Immunofluorescence staining (as indicated) of zygotes derived from WT and *Lsm14b* knockout mice mated with WT males. Scale bar = 20 μm. (**I**) The rates of one pronuclear (1PN) and 2PN zygotes collected from WT and *Lsm14b* knockout mice. The numbers of analyzed oocytes are indicated (*n*). Data are presented as the mean ± SEM. $^{****}P < 0.0001$. (**J**) Quantification of pre-implantation embryos derived from WT and *Lsm14b* knockout mice. The numbers of analyzed embryos are indicated (*n*). Data are presented as the mean ± SEM. $^{***}P < 0.001$ and $^{****}P < 0.0001$. (**K**) Schematic for WT and *Lsm14b* knockout oocyte meiotic maturation and early embryogenesis.

with hyaluronidase (300 IU/ml). The rates of PB1 emission in *Lsm14b* knockout oocytes were comparable with those in the control group (Figure 2E), and the number of oocytes ovulated was also comparable (Figure 2D).

To our surprise, 61.17% of the ovulated oocytes from the *Lsm14b* knockout mice collected 16 h after hCG injection had a first polar body (PB1) and an 'interphase-like nucleus', and 32.29% of the ovulated oocytes from the *Lsm14b* knockout mice collected 14 h after hCG injection had a PB1 and an 'interphase-like nucleus' (Figure 2A, F). Immunofluorescence, in combination with confocal microscopy, demonstrated that the *Lsm14b* knockout oocytes exhibited typical PB1 emission, but did not transition to meiosis II. Instead, these oocytes underwent chromosomal decondensation, accompanied by the development of interphase-like nuclei (Figure 2A, B). Importantly, when we retrieved oocytes at 14 h after hCG injection and cultured them for 72 h *in vitro*, none of the oocytes from *Lsm14b* knockout mice developed further (Supplementary Figure S1A). These findings together indicate that loss of LSM14B function does not lead to activation of parthenogenesis; rather, the defect in the *Lsm14b* knockout oocytes occurs in meiosis. So, although the resumption of oocyte meiosis I can occur in the absence of LSM14B, LSM14B is required for normal progression to MII.

Lsm14b knockout oocytes display impaired early embryogenesis

We mated superovulated *Lsm14b* knockout female mice with WT male mice to assess fertilization in detail. This produced a small number of two-cell embryos, but no four-cell embryos, eight-cell embryos or blastocysts (Figure 2G, J), so we conducted immunofluorescence staining on zygotes (Figure 2H). About 80% of the zygotes from *Lsm14b* knockout mice exhibited abnormal monopronuclear (1PN) states, a significantly higher proportion than observed for zygotes from WT mice (∼18%). In contrast, the percentage of normal bipronuclear (2PN) state zygotes from WT mice was 84%, while it was only ∼22% from the *Lsm14b* knockout mice (Figure 2I). We then used an EU incorporation assay to profile transcription activity of the 2PN state zygotes derived from *Lsm14b* knockout mice (using GV stage oocytes collected from the WT as a negative control). EU signals were decreased in *Lsm14b* knockout 2PN zygotes (Supplementary Figure S1B, C). The results indicate that the knockout of *Lsm14b* in mice affects the entry into MII, leading to the occurrence of fertilization reproductive defects.

LSM14B deletion disrupts mitochondrial clustering in oocytes and impairs energy metabolism

Following synthesis in the oocyte, maternal mRNAs are translationally silenced and sequestered into storage incytoplasmic granules (28). Thus it is critical for oocyte maturation and early embryonic development to store the maternal mRNAs properly. Previous studies have indicated that LSM14, a member of the like-Sm (LSM) protein family, is highly conserved from yeast to humans and it is one of the key components in the assembly of the mammalian gene silencing complexes (22). Recent studies discovered a new domain, a mitochondria-associated membraneless compartment that stores maternal mRNAs in oocytes of various mammalian species, named MARDO (mitochondria-associated ribonucleoprotein domain) (2). Speculation about the existence of structural and functional connections between LSM14B and MARDO piqued our interest.

To verify this speculation, we generated *Lsm14b*-mCherry mRNA. Then we expressed LSM14B in the WT oocytes at different stages by microinjection with *Lsm14b*-mCherry mRNA and found that LSM14B co-localized with mitochondria stained with MitoTracker (Figure 3A). The co-localization of LSM14B and mitochondria reached its highest level at the MI stage. The co-localization between LSM14B and the mitochondrial marker HSP60 shows the same phenomenon (Supplementary Figure S2A, B). In addition, co-localization was not detected in NSN stage oocytes (Figure 3B). These results suggest that with the maturation of oocytes, the co-localization of LSM14B and mitochondria gradually strengthened. The co-localization of LSM14B and mitochondria indicated that LSM14B may be involved in the formation of MARDO (2).

We also performed immunostaining for mitochondria with MitoTracker on live oocytes derived from WT and *Lsm14b* knockout mice at different growth stages and assessed the mitochondrial distribution: GV stage oocytes with LSM14B deletion shifted from a uniform distribution around the GV (Figure 3C, D) to a subcortical accumulation pattern (Figure 3C, E). Further, the proportion of abnormally distributed mitochondria reached as high as 80% in GV stage oocytes from *Lsm14b* knockout mice (Figure 3I).

Consistent with previous studies of MI (2), our data show when we depleted LSM14B by gene knockout, the mitochondrial clustering was impaired (Figure 3F). Specifically, the mitochondrial distribution in MI stage oocytes with LSM14B deletion shifted from the state of clustering around the spindle (Figure 3G) to the uniform distribution around the GV (Figure 3H). Also 81% of *Lsm14b* knockout MI stage oocytes showed an abnormal distribution of mitochondria, without formation of a mitochondrial ring (Figure 3I). Additionally, RNA-FISH indicated that poly(A)-positive mRNAs associated with the mitochondria are no longer associated in the *Lsm14b* knockout oocyte (Figure 3L). These results demonstrate that LSM14B deletion disrupts MARDO and mitochondrial clustering in oocytes.

Maternal mitochondria provide the ATP needed for oocyte meiotic maturation and early embryonic development using oxidative phosphorylation (OXPHOS) (31,32); however, active OXPHOS tends to drives ROS generation, which is associated with lower rates of fertilization and embryo survival (33,34). We measured ATP and ROS levels in GV and MII (14 h after hCG injection) oocytes derived from WT and *Lsm14b* knockout mice. As expected, deletion of LSM14B results in a decreased level of ATP and an increased level in ROS in both the GV stage oocytes and MII (14 h after hCG injection) stage oocytes (Figure 3J, K). Together, our data indicate that LSM14B has impacts on mitochondrial clustering and energy metabolism.

Transcriptome analysis indicates decreases in maternal mRNA storage in *Lsm14b* knockout oocytes

We investigated the intrinsic factors that affect the meiotic maturation of oocytes by performing mRNA sequencing analysis of GV and MII stage oocytes derived from WT and *Lsm14b* knockout mice (Figure 4A). Scatter plots of RNA-seq data illustrate transcriptional changes in *Lsm14b* knockout oocytes at the GV and MII stage. Compared with GV stage oocytes of WT mice, the levels of 1805 and 1340 transcripts were respectively increased or decreased in the GV stage oocytes of *Lsm14b* knockout mice (by >2-fold) (Figure 4B, left panel). With meiosis progression to the MII stage, a larger number of transcripts displayed changes between the *Lsm14b* knockout and WT oocytes, with 2302 up-regulated and 1939 down-regulated transcripts in the *Lsm14b* knockout samples (Figure 4B, right panel).

We further performed GO analyses of the transcripts that decreased in *Lsm14b* knockout oocytes at the GV and MII stages. The down-regulated transcripts in the GV stage of *Lsm14b* knockout mice were enriched for terms related to transcription initiation and regulation of the cell cycle (Figure 4C). In MII stage oocytes of *Lsm14b* knockout mice, the down-regulated transcripts were enriched in terms related to translation ('RNA splicing', 'regulation of translation', 'mRNA processing' and 'regulation of RNA stability') (Figure 4D). qPCR verified that several mRNAs with known mitochondria-related and RNA processing- and decay-related functions were decreased in *Lsm14b* knockout GV stage oocytes (Figure 4E). The decreases in transcripts encoding regulators of mRNA stability drew our particular attention as recent studies have indicated that incomplete maternal mRNA decay during the MZT can drive pre-implantation developmental arrest (35). Therefore, we hypothesized that the inability for maternal mRNA degradation during oocyte

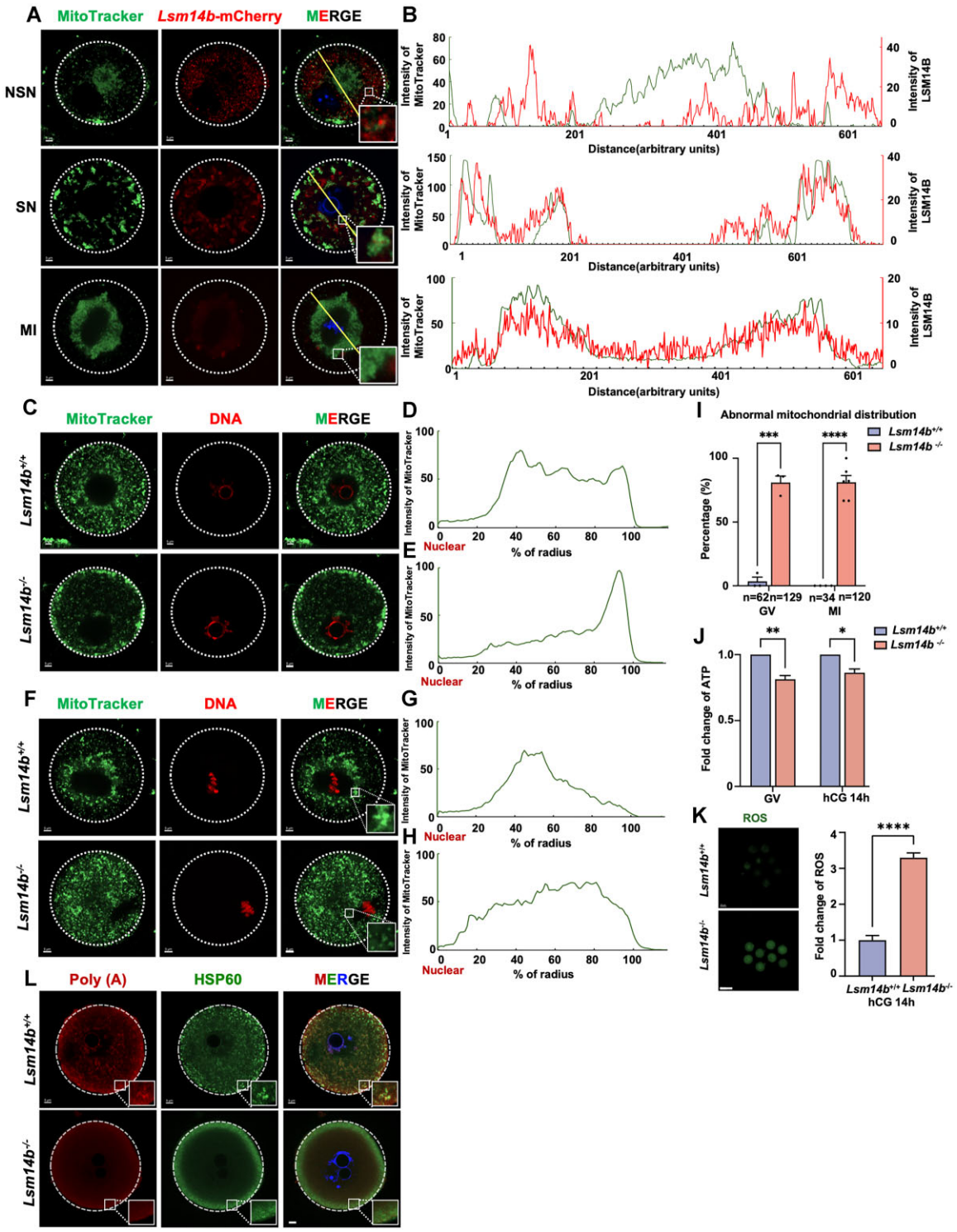

Figure 3. The distribution and function of mitochondria are impaired in *Lsm14b* knockout oocytes. (**A**) Representative immunofluorescence images of mouse oocytes at the indicated growth stages. *Lsm14b*-mCherry (red), counterstained with MitoTracker (green). Insets are magnifications of outlined regions. The dashed line demarcates the oocyte. Scale bar = 5 μm. (**B**) Intensity profiles along the yellow lines in (A). (**C**) Representative immunofluorescence images of GV stage oocytes collected from WT and *Lsm14b* knockout mice. The dashed line demarcates the oocyte. Scale bar = 5 μm. (**D** and **E**) ImageJ was used to quantitatively analyze the distribution of mitochondria in (C). (**F**) Representative immunofluorescence images of MI stage oocytes collected from WT and *Lsm14b* knockout mice. Insets are magnifications of outlined regions. The dashed line demarcates the oocyte. Scale bar = 5 μm. (**G** and **H**) ImageJ was used to quantitatively analyze the distribution of mitochondria in (F). (**I**) Rates of abnormal distribution of mitochondria in GV and MI stage oocytes. The number of analyzed embryos is indicated (*n*). Error bars show the SEM. $^{***}P < 0.001$ and $^{****}P < 0.0001$ by two-tailed Student's *t*-tests. (**J**) ATP content in WT and *Lsm14b* knockout oocytes. Error bars show the SEM. $^{*}P < 0.05$ and $^{**}P < 0.01$ by two-tailed Student's *t*-tests. (**K**) Representative images and quantification of CM-H2DCFDA fluorescence (green) in WT and *Lsm14b* knockout oocytes. Scale bar = 100 μm. Error bars show the SEM. $^{****}P < 0.0001$ by two-tailed Student's *t*-tests. (**L**) Representative RNA-FISH images of mouse GV oocytes collected from WT and *Lsm14b* knockout mice. mRNAs with a poly(A) tail (red), counterstained with HSP60 (green). Insets are magnifications of outlined regions. The dashed line demarcates the oocyte. Scale bar = 5 μm.

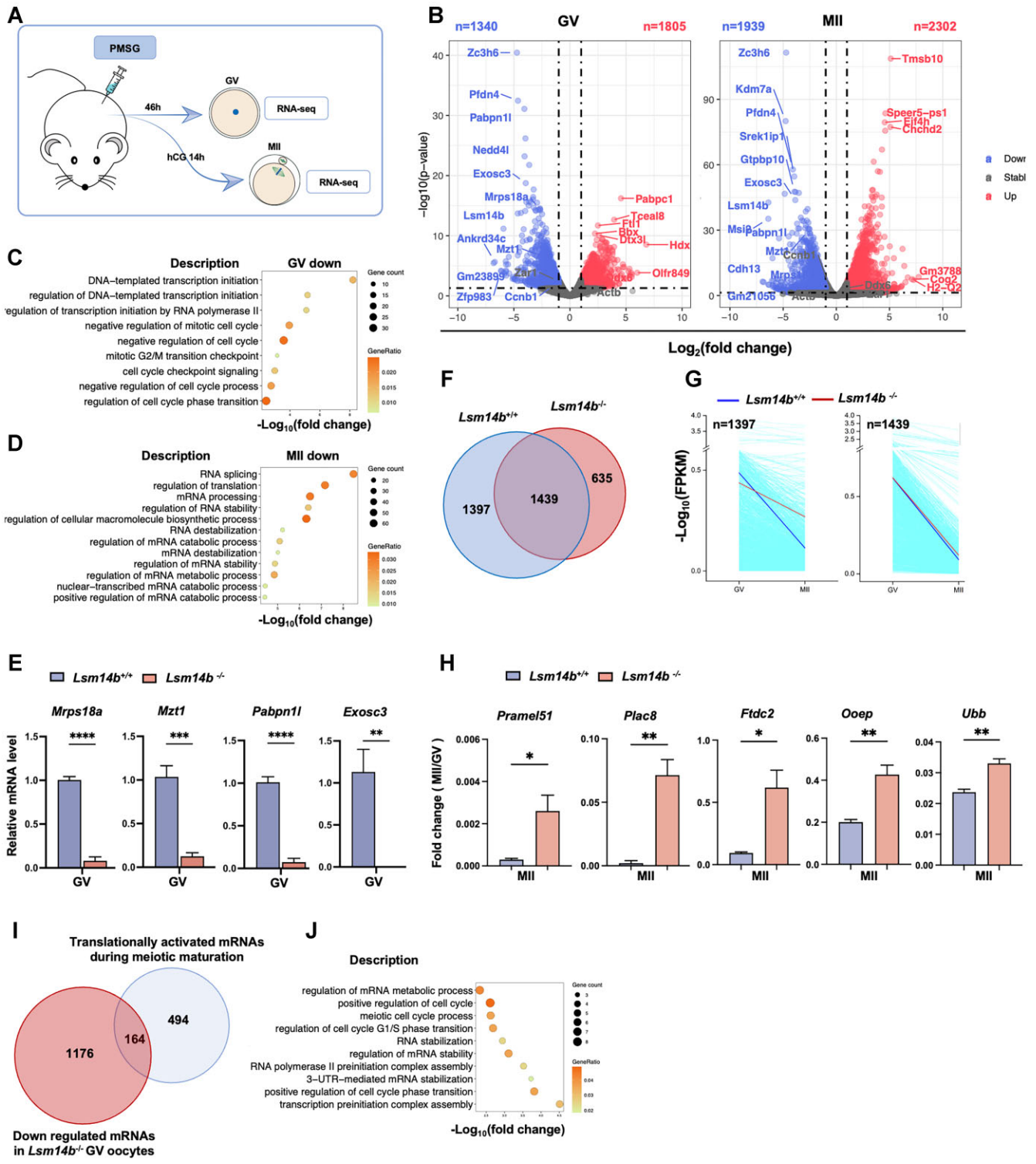

Figure 4. Maternal mRNA storage and clearance are defective in *Lsm14b* knockout oocytes. (**A**) Schematic for samples examined with RNA-seq. (**B**) Volcano plot comparing the transcripts of oocytes from WT and *Lsm14b* knockout mice (GV, MII stage oocytes). Transcripts that increased or decreased by >2-fold in *Lsm14b* knockout oocytes are highlighted in red or blue, respectively. (**C** and **D**) Bubble charts showing the down-regulated genes in GV and MII stage oocytes. (**E**) qPCR results showing expression levels of mRNAs encoding *Mrps18a*, *Mzt1*, *Pabpn1l* and *Exosc3* in GV stage oocytes. Error bars shown the SEM. $^{**}P < 0.01$, $^{***}P < 0.001$ and $^{****}P < 0.0001$ by two-tailed Student's *t*-tests. (**F**) Venn diagram showing the overlap of M-decay transcripts (decreased 4-fold from the GV to MII stage) in oocytes from WT and *Lsm14b* knockout mice. (**G**) Degradation patterns of maternal transcripts during the GV–MII transition in oocytes derived from WT and *Lsm14b* knockout mice. Each teal line represents the expression levels of one gene, and the middle red and blue lines represent the median expression levels of the two groups. (**H**) qPCR results for FCs of the indicated maternal transcripts in oocytes at the MII stage from WT and *Lsm14b* knockout females. Error bars show the SEM. $^{*}P < 0.05$ and $^{**}P < 0.01$ by two-tailed Student's *t*-tests. (**I**) Venn diagrams showing the overlap in transcripts. Cyan, translationally activated mRNAs during oocyte meiotic maturation; red, down-regulated mRNAs in *Lsm14b* knockout GV oocytes, $\log_2$FC < –1 (*Lsm14b* knockout versus WT oocytes). (**J**) Bubble charts showing the down-regulated genes in GV stage oocytes.

meiotic maturation is a key factor to obstruct the embryogenesis in *Lsm14b* knockout mice.

To test this hypothesis, we analyzed the transcriptome changes in GV–MII stage oocytes that apparently underwent large-scale mRNA M-decay during meiotic maturation between WT and *Lsm14b* knockout mice. In WT oocytes, 2836 transcripts were significantly degraded during the GV–MII transition [FC(GV/MII) > 4]. A total of 2074 transcripts were significantly degraded during the GV–MII transition in *Lsm14b* knockout oocytes [FC(GV/MII) > 4]. Furthermore, the transcripts showed a significant overlap (Figure 4F). We further divided the 2836 M-decay transcripts of WT oocytes into two groups: those sensitive to LSM14B deletion (1397; those transcripts which were not degraded in *Lsm14b* knockout oocytes) and those insensitive to LSM14B deletion (1439; those transcripts where degradation in oocytes was not affected by LSM14B deletion). The degradation pattern showed that the transcripts that are sensitive to LSM14B deletion in *Lsm14b* knockout oocytes were lower than those in WT mice at the GV stage, but remained relatively stable during meiotic maturation, and ended up with higher levels than in WT oocytes at the MII stage (Figure 4G, left panel). The transcripts that were insensitive to LSM14B deletion in *Lsm14b* knockout oocytes had comparable levels with those of WT oocytes at the GV stage, and were degraded during GV–MII transition, albeit to a lesser extent compared with WT oocytes (Figure 4G, right panel). Using qPCR, we confirmed that the selected maternal transcripts were degraded during WT oocyte maturation but were stabilized in *Lsm14b* knockout oocytes (Figure 4H).

Recall that many mRNAs are stored in special structure during oocyte growth and are translationally activated when the oocyte resumes meiosis. To identify whether LSM14B knockout affects the translational activation during oocyte meiotic maturation, we re-analyzed the 1340 down-regulated transcripts of the GV stage of *Lsm14b* knockout oocytes as compared with WT oocytes by combining with Gene Expression Omnibus (GEO) accession number GSE135525 (36). We found that 164 transcripts were prematurely lost in *Lsm14b* knockout oocytes (Figure 4I). Notably, a GO analysis indicated that this set of genes was enriched for regulation of the cell cycle and for transcription initiation-related functions, such as regulation of RNA stabilization and mRNA metabolic process (Figure 4J).

These results demonstrate that loss of LSM14B function disrupts mRNA storage and clearance.

LSM14B deletion causes down-regulation of proteins related to mRNA storage and stability

Considering that the combined use of transcriptomics and proteomics is usually more accurate than the use of transcriptomics alone, we examined proteomics for further analysis to characterize the factors which have an influence during oocyte maturation. The sample collection method is as shown in Figure 5A.

Scatter plots of proteomics data illustrated translational changes in *Lsm14b* knockout oocytes (MII). Compared with oocytes (MII) derived from WT mice, 107 and 103 proteins were increased or decreased by > 1.5-fold in the oocytes (MII) of *Lsm14b* knockout mice. Among the significantly down-regulated proteins, several kinds of proteins have caught our attention, including DDX6, ZAR1 and EIF4ENIF1, which are involved in the formation of MARDO (2). Cyclin B1 (CCNB1 for short) and BTG4 were also notable, as these function in cell cycle progression and mRNA M-decay (Figure 5B).

MARDO, is a mitochondria-associated membraneless compartment that stores maternal mRNAs in oocytes of various mammalian species. The RNA-binding protein ZAR1 promotes MARDO assembly, and DDX6 is also a component of MARDO (2). The deletion of LSM14B resulted in a sharp decrease in the protein levels of ZAR1 and DDX6 (Figure 5F, G). Further, we demonstrated that ZAR1 co-precipitated with LSM14B in HeLa cells, but their interaction was weakened by RNase A treatment, indicating that there are other molecules besides RNA for interaction between LSM14B and ZAR1 (Figure 5J). GSEA data revealed that pathways associated with mitochondrial electron transport, ATP synthesis and the NADH dehydrogenase complex were significantly up-regulated in the control group, while this phenomenon did not exist in the LSM14B knockout group (Figure 5C). These results were consistent with our previous findings that LSM14B deletion impairs energy metabolism (Figure 3J, K). Collectively, the experimental data once again demonstrated that the deletion of LSM14B has an impact on MADRO and mitochondrial function.

To further investigate the potential role of LSM14B in mRNA storage and decay during meiosis maturation, we selected 3165 transcripts that were up- or down-regulated >2-fold in *Lsm14b* knockout GV stage oocytes compared with WT oocytes. Also 103 translations that were 1.5-fold down-regulated in *Lsm14b* knockout oocytes (MII) compared with WT oocytes (MII) were selected. The results show that there is a meaningful overlap between Cyclin B1 and BTG4 (Figure 5D). The RNA-FISH results showed that the mRNAs encoding *Btg4* and *CyclinB1* no longer aggregated in *Lsm14b* knockout oocytes (Figure 5E). The complex protein Cyclin B1 regulates CDK1 activity, and is understood to be the regulatory subunit. Immunoblotting demonstrated that the expression level of Cyclin B1 was significantly decreased when LSM14B was deleted (Figure 5H). The synthesis and degradation of Cyclin B1 regulates a sequence of events during meiotic progression, including GV arrest, GVBD, the metaphase–anaphase transition of the first meiosis and the metaphase arrest/exit of the second meiosis (37). BTG4 as a meiotic cell cycle-coupled MZT licensing factor that triggers decay of maternal mRNA in maturing mammalian oocytes (10). In addition to the interaction between LSM14B and proteins necessary for maternal mRNA metabolism and oocyte development, we also examined the potential effects of LSM14B on translation initiation and regulatory factoris by western blot. *Lsm14b* knockout reduced the protein levels of EIF4E1B and EIF4ENIF1 (Figure 5I).

Collectively, these results, together with our observation of decreased Cyclin B1 and BTG4 proteomics levels in *Lsm14b* knockout oocytes, demonstrate that LSM14B is required for the storage and stability of mRNAs encoding Cyclin B1 and BTG4 by participating in the formation of MARDO.

Exogenous supplementation of *Lsm14b* and *Zar1* mRNA rescues mitochondrial distribution defects

We further assessed the involvement of LSM14B in MARDO assembly by generating *Lsm14b*-mCherry and *Zar1*-Flag mRNA, and then performed microinjection into GV stage oocytes of *Lsm14b* knockout mice to express LSM14B and

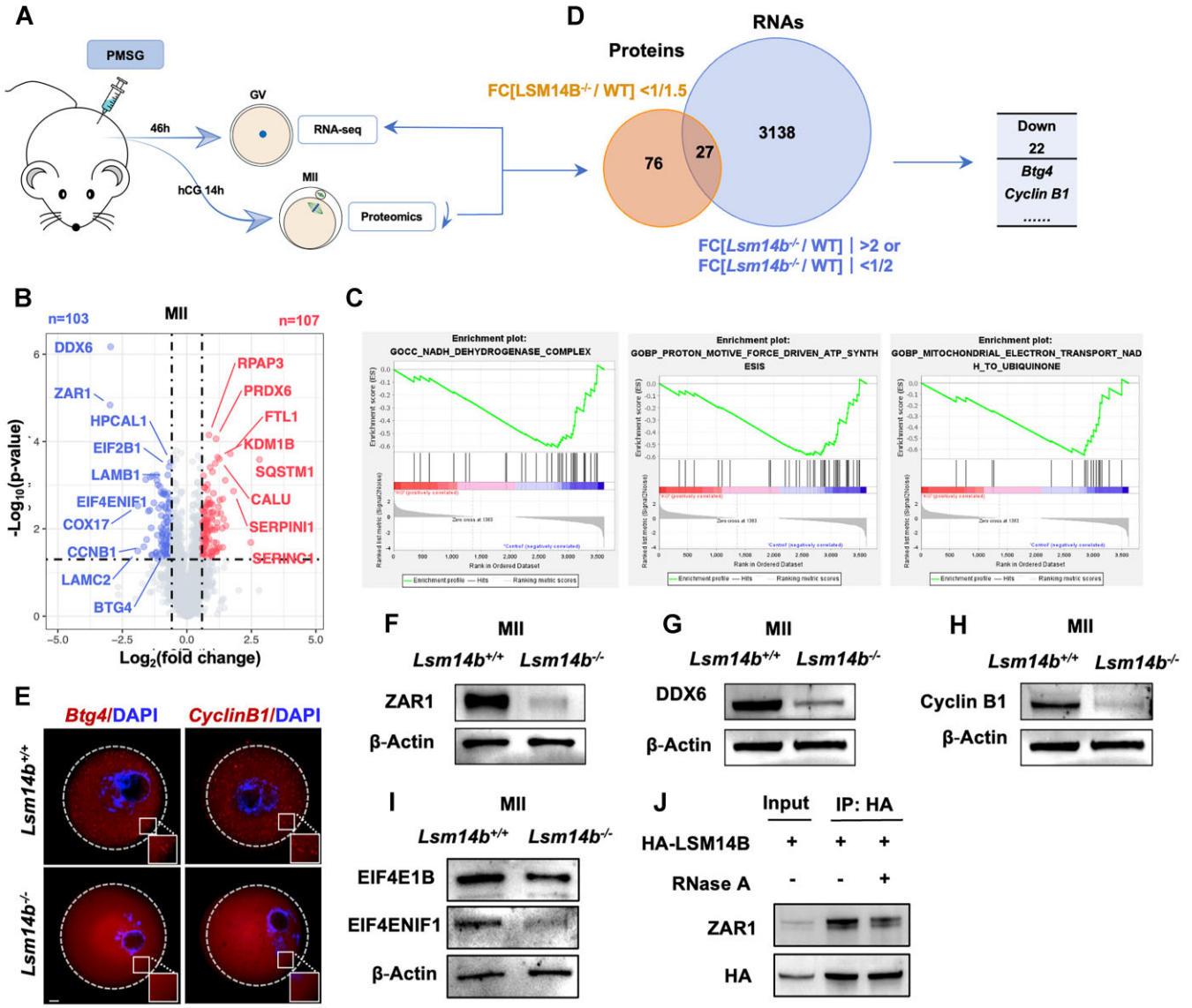

Figure 5. LSM14B deletion causes down-regulation of proteins with functions in meiosis maturation and early embryo development. (**A**) Schematic for samples examined with proteomics. (**B**) Volcano plot comparing the proteins of WT and *Lsm14b* knockout oocytes at the MII stage (14 h after hCG injection). Proteins that increased or decreased by >2-fold in *Lsm14b* knockout oocytes are highlighted in red or blue, respectively. (**C**) The three enrichment plots from the GSEA results. (**D**) Venn diagrams showing the overlap in proteomics. Orange, down-regulated proteins in *Lsm14b* knockout MII oocytes (1.5 FC, *Lsm14b* knockout versus WT oocytes). Blue, up- and down-regulated transcripts in *Lsm14b* knockout GV oocytes (>2 FC, *Lsm14b* knockout versus WT oocytes). (**E**) Representative RNA-FISH images of mouse GV oocytes collected from WT and *Lsm14b* knockout mice. *Btg4* and *CyclinB1* were labeled with 5′-Cy3-Oligo d(T)30. Insets are magnifications of outlined regions. The dashed line demarcates the oocyte. Scale bar = 5 μm. (**F**) Immunoblotting against ZAR1 in MII stage oocytes derived from WT and *Lsm14b* knockout mice; β-actin was used as the protein loading control. (**G**) Immunoblotting against DDX6 in MII stage oocytes derived from WT and *Lsm14b* knockout mice; β-actin was used as the protein loading control. (**H**) Immunoblotting against Cyclin B1 in MII stage oocytes derived from WT and *Lsm14b* knockout mice; β-actin was used as the protein loading control. (**I**) Immunoblotting against EIF4ENIF1 and EIF4E1B in MII stage oocytes derived from WT and *Lsm14b* knockout mice; β-actin was used as the protein loading control. (**J**) Co-IP and immunoblotting results showing the interaction between LSM14B and ZAR1. HeLa cells were transiently transfected with plasmids expressing the indicated proteins, and were harvested for Co-IP at 48 h after plasmid transfection.

ZAR1. LSM14B co-localized with ZAR1, and oocytes with exogenous *Lsm14b* expression regain a normal ZAR1 signal at subcortical aggregates (Figure 6A–E).

Considering the obviously decreased protein level of ZAR1 in *Lsm14b* knockout oocytes, we explored whether microinjecting *Lsm14b* and *Zar1* mRNA could rescue the mitochondrial distribution defects of *Lsm14b* knockout oocytes that were arrested at the GV stage using milrinone. After their release from milrinone, oocytes were stained with MitoTracker directly or cultured for 8 h (Figure 6F). Consistent with the GV oocytes without exogenous mRNA supplementation, none of the distribution pattern of mitochondria was rescued in GV oocytes with microinjection of *Lsm14b* and *Zar1*, respectively, or of both *Lsm14b* and *Zar1* (Figure 6F, G). Conversely, mitochondria have regained their normal distribution pattern enriched at the spindle periphery in MI stage *Lsm14b* knockout oocytes after exogenous *Lsm14b* and *Zar1* mRNA supplementation (Figure 6G–I). Collectively, overexpression of LSM14B and ZAR1 in oocytes significantly rescued the impaired mitochondrial distribution in *Lsm14b* knockout

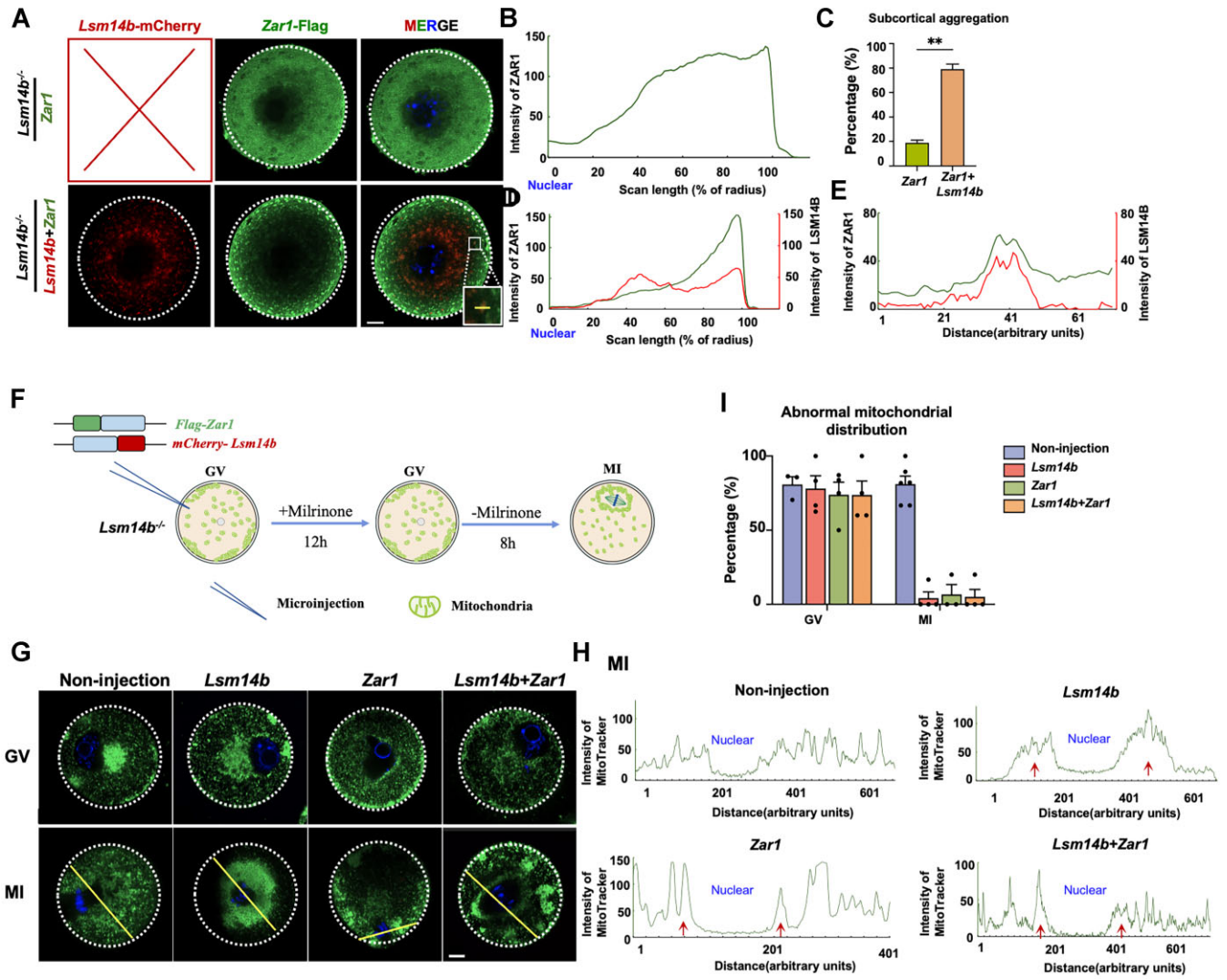

Figure 6. Exogenous supplementation of *Lsm14b* and *Zar1* mRNA rescues mitochondrial distribution defects. (**A**) ZAR1 and LSM14B immunofluorescence results in GV stage oocytes of *Lsm14b* knockout mice. Scale bar = 10 μm. (**B**) ImageJ was used to quantitatively analyze the intensity of ZAR1 in (A). (**C**) Rates of the subcortical aggregation pattern of ZAR1 in *Lsm14b* knockout oocytes. Error bars show the SEM. $^{**}P < 0.01$ by two-tailed Student's *t*-tests. (**D**) ImageJ was used to quantitatively analyze the intensity of ZAR1 and LSM14B in (A). (**E**) Intensity profiles of ZAR1 and LSM14B along the yellow lines in (A). (**F**) Schematic of the procedure for the rescue experiment. (**G**) Representative immunofluorescence images of the mitochondrial distribution in *Lsm14b* knockout oocytes with injection at different growth stages. Scale bar = 10 μm. (**H**) Intensity profiles of mitochondria along the yellow lines in (G). The clusters of mitochondria are indicated by the red arrowhead. (**I**) Rates for an abnormal mitochondrial distribution in GV and MI stage oocytes of *Lsm14b* knockout mice.

MI stage oocytes. These results suggest that the loss of LSM14B disrupts the MARDO and mitochondrial clustering, while restoration of *Lsm14b* can rescue the aforementioned abnormalities.

Discussion

We have demonstrated that LSM14B is essential for oocyte meiotic maturation and observed that female mice lacking functional LSM14B are infertile. With *Lsm14b* knockout mice, we have shown that LSM14B functions in ensuring the proper accumulation and clearance of mRNAs essential for oocyte meiotic maturation, successive transition of meiosis I and meiosis II, and subsequent early embryogenesis. Our rescue data for MARDO assembly and the mitochondrial distribution in *Lsm14b* knockout oocytes based on *Lsm14b* mRNA microinjection support that LSM14B is essential for MARDO assembly, thus deepening understanding about the formation and functions of this compartment (Figure 7).

After oocyte meiotic resumption, transcriptional quiescence ensues, so the correct translation and timely M-decay of prestored mRNAs is understood as essential for oocyte competence (4,10). Our results showed that LSM14B promoted the correct accumulation and clearance of mRNAs in oocytes. Of particular note, in *Lsm14b* knockout oocytes, the storage of *Btg4* and *Cyclin B1* in GV oocytes was disrupted, and the BTG4 and Cyclin B1 protein levels in MII oocytes were decreased. Previous research has shown that BTG4 facilitates CCR4–NOT-mediated mRNA decay by shortening the poly(A) tails of mRNAs at the meiosis I and meiosis II transition and demonstrated that this wave of deadenylation is essential for inhibition of the APC/C complex and for the re-accumulation of Cyclin B1 for entry to meiosis II (10,20). Our findings are consistent with those of Li *et al.*, who reported

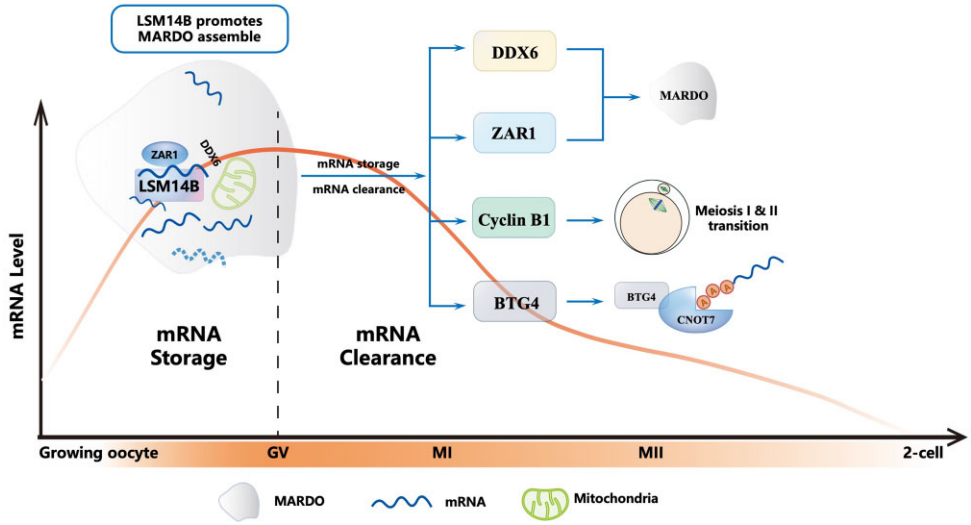

Figure 7. A model for LSM14B's role in regulating mRNA storage and clearance in oocytes. In GV oocytes, LSM14B promotes MARDO assembly together with ZAR1 and DDX6 to function in mRNA storage and clearance (including *Cyclin B1*, *Btg4* and other mRNAs that become translationally activated) during oocyte meiotic maturation.

that Cyclin B1 knockout oocytes entered an interphase-like phase after PB1 extrusion, without arrest at MII in mice (38). It is notable that our RNA-seq dataset shows that the storage and degradation of a subset of maternal mRNAs are affected by LSM14B during oocyte meiotic maturation. Su *et al*. conducted LACE-seq (linear amplification of cDNA ends and sequencing) and found that LSM14B binds to multiple mRNAs necessary for oocyte nuclear and cytoplasmic maturation (e.g. *Ybx2* and *Patl2*) and follicle developmental regulatory factors (e.g. *Gdf9* and *Grp3*) (39). However, further investigations will be needed to determine the mechanism(s) through which LSM14B specifically regulates these mRNAs.

MARDO assembly occurs in NSN oocytes, and this compartment is most prominently evident in MI oocytes (2). Previous reports showed that ZAR1 was enriched in the cortical region of growing oocytes (40) and demonstrated that ZAR1 is essential for MARDO assembly (2). We found that LSM14B functions in promoting MARDO assembly, and specifically show that LSM14B co-localizes with ZAR1 to facilitate its cortical distribution in an RNA-mediated manner. Besides LSM14B's role in mRNA storage through contributing to MARDO assembly, our study has preliminarily indicated a potential role for LSM14B in mRNA degradation *per se*; however, further evidence will be required to demonstrate the mechanisms of degradation-specific functions. Intriguingly, this would be reminiscent of another mRNA reservoir and clearance structure in early growing oocytes, P-bodies, so it is notable that LSM14B is known to be an essential constituent for the integrity of that compartment (39,41–43). In addition to proteins that are involved in RNA binding, P-bodies include proteins with roles in RNA interference and translational repression (43,44). However, as mice oocytes grow larger, P-bodies disperse as MARDO assembly begins in NSN oocytes (2,42,45,46). Whether MARDO has similar functions in oocytes remains to be investigated.

Data availability

The RNA-seq data have been deposited in the NCBI Gene Expression Omnibus database with the GEO accession number GSE231648. The proteomics data are available in the Proteome Xchange database with the accession number PXD042761.

Supplementary data

Supplementary Data are available at NAR Online.

Acknowledgements

We thank all our colleagues in the Chen laboratory for helpful discussions.

Author contributions: H.B.L., Q.Q.S. and Z.J.C. designed the study and provided valuable contributions to the whole study. Y.L.W. and S.Y. performed most of the experiments. T.T.L. analyzed the proteomics data. Y.L.C. performed the LACE-seq experiments. M.Y.Z. performed genotyping. X.Y.W., T.M., T.H., Y.L., W.-Y.C., G.L. and J.X.L. critically reviewed the manuscript. All authors read and approved the final manuscript.

Funding

The National Key Research and Development Program of China [2022YFC2703200]; Basic Science Center Program of the NFSC [31988101]; National Key R&D Program of China [2021YFC2700200]; Academic Promotion Programme of Shandong First Medical University [2019U001]; National Key Research and Development Program of China [2021YFC2700100]; the National Natural Science Foundation of China [82101731 and 81771538];Research Unit of Gametogenesis and Health of ART-Offspring, Chinese Academy of Medical Sciences [2020RU001]; the Research Grants Council of Hong Kong [14103418]; the Shandong Provincial Key Research and Development Program [2020ZLYS02]; the A-Smart Group to support the CUHK-SDU Joint Laboratory on Reproductive Genetics of CUHK [690598 and 8601534]; Major Innovation Projects in Shandong Province [2021ZDSYS16]; the Science Foundation for Distinguished Yong Scholars of Shandong [ZR2021JQ27];

and Taishan Scholars Program for Young Experts of Shandong Province [tsqn202103192].

Conflict of interest statement

None declared.

References

1. Zheng,W., Zhou,Z., Sha,Q., Niu,X., Sun,X., Shi,J., Zhao,L., Zhang,S., Dai,J., Cai,S., *et al.* (2020) Homozygous mutations in BTG4 cause zygotic cleavage failure and female infertility. *Am. J. Hum. Genet.*, **107**, 24–33.
2. Cheng,S., Altmeppen,G., So,C., Welp,L.M., Penir,S., Ruhwedel,T., Menelaou,K., Harasimov,K., Stützer,A., Blayney,M., *et al.* (2022) Mammalian oocytes store mRNAs in a mitochondria-associated membraneless compartment. *Science*, **378**, eabq4835.
3. Sha,Q.Q., Zhang,J. and Fan,H.Y. (2019) A story of birth and death: mRNA translation and clearance at the onset of maternal-to-zygotic transition in mammals. *Biol. Reprod.*, **101**, 579–590.
4. Liu,Y., Lu,X., Shi,J., Yu,X., Zhang,X., Zhu,K., Yi,Z., Duan,E. and Li,L. (2016) BTG4 is a key regulator for maternal mRNA clearance during mouse early embryogenesis. *J. Mol. Cell Biol.*, **8**, 366–368.
5. Jiang,Y., Adhikari,D., Li,C. and Zhou,X. (2023) Spatiotemporal regulation of maternal mRNAs during vertebrate oocyte meiotic maturation. *Biol. Rev. Camb. Philos. Soc.*, **98**, 900–930.
6. Hu,W., Zeng,H., Shi,Y., Zhou,C., Huang,J., Jia,L., Xu,S., Feng,X., Zeng,Y., Xiong,T., *et al.* (2022) Single-cell transcriptome and translatome dual-omics reveals potential mechanisms of human oocyte maturation. *Nat. Commun.*, **13**, 5114.
7. Fluks,M., Szczepanska,K., Ishikawa,T. and Ajduk,A. (2019) Transcriptional status of mouse oocytes corresponds with their ability to generate Ca2+ release. *Reproduction*, **157**, 465–474.
8. Monti,M., Zanoni,M., Calligaro,A., Ko,M.S., Mauri,P. and Redi,C.A. (2013) Developmental arrest and mouse antral not-surrounded nucleolus oocytes. *Biol. Reprod.*, **88**, 2.
9. Dai,X.X., Jiang,J.C., Sha,Q.Q., Jiang,Y., Ou,X.H. and Fan,H.Y. (2019) A combinatorial code for mRNA 3'-UTR-mediated translational control in the mouse oocyte. *Nucleic Acids Res.*, **47**, 328–340.
10. Yu,C., Ji,S.Y., Sha,Q.Q., Dang,Y., Zhou,J.J., Zhang,Y.L., Liu,Y., Wang,Z.W., Hu,B., Sun,Q.Y., *et al.* (2016) BTG4 is a meiotic cell cycle-coupled maternal–zygotic-transition licensing factor in oocytes. *Nat. Struct. Mol. Biol.*, **23**, 387–394.
11. Luong,X.G., Daldello,E.M., Rajkovic,G., Yang,C.R. and Conti,M. (2020) Genome-wide analysis reveals a switch in the translational program upon oocyte meiotic resumption. *Nucleic Acids Res.*, **48**, 3257–3276.
12. Sha,Q.Q., Yu,J.L., Guo,J.X., Dai,X.X., Jiang,J.C., Zhang,Y.L., Yu,C., Ji,S.Y., Jiang,Y., Zhang,S.Y., *et al.* (2018) CNOT6L couples the selective degradation of maternal transcripts to meiotic cell cycle progression in mouse oocyte. *EMBO J.*, **37**, e99333.
13. Wu,D. and Dean,J. (2016) BTG4, a maternal mRNA cleaner. *J. Mol. Cell Biol.*, **8**, 369–370.
14. Jones,K.T. (2004) Turning it on and off: M-phase promoting factor during meiotic maturation and fertilization. *Mol. Hum. Reprod.*, **10**, 1–5.
15. Jiang,J.C., Zhang,H., Cao,L.R., Dai,X.X., Zhao,L.W., Liu,H.B. and Fan,H.Y. (2021) Oocyte meiosis-coupled poly(A) polymerase α phosphorylation and activation trigger maternal mRNA translation in mice. *Nucleic Acids Res.*, **49**, 5867–5880.
16. Roeder,G.S. (1997) Meiotic chromosomes: it takes two to tango. *Genes Dev.*, **11**, 2600–2621.
17. Loidl,J. (2016) Conservation and variability of meiosis across the eukaryotes. *Annu. Rev. Genet.*, **50**, 293–316.
18. Polański,Z., Homer,H. and Kubiak,J.Z. (2012) Cyclin B in mouse oocytes and embryos: importance for human reproduction and aneuploidy. *Results Probl. Cell Differ.*, **55**, 69–91.
19. Sun,Q.Y., Miao,Y.L. and Schatten,H. (2009) Towards a new understanding on the regulation of mammalian oocyte meiosis resumption. *Cell Cycle*, **8**, 2741–2747.
20. Pasternak,M., Pfender,S., Santhanam,B. and Schuh,M. (2016) The BTG4 and CAF1 complex prevents the spontaneous activation of eggs by deadenylating maternal mRNAs. *Open Biol*, **6**, 160184.
21. Ledan,E., Polanski,Z., Terret,M.E. and Maro,B. (2001) Meiotic maturation of the mouse oocyte requires an equilibrium between cyclin B synthesis and degradation. *Dev. Biol.*, **232**, 400–413.
22. Marnef,A., Sommerville,J. and Ladomery,M.R. (2009) RAP55: insights into an evolutionarily conserved protein family. *Int. J. Biochem. Cell Biol.*, **41**, 977–981.
23. Albrecht,M. and Lengauer,T. (2004) Novel Sm-like proteins with long C-terminal tails and associated methyltransferases. *FEBS Lett.*, **569**, 18–26.
24. Mura,C., Phillips,M., Kozhukhovsky,A. and Eisenberg,D. (2003) Structure and assembly of an augmented Sm-like archaeal protein 14-mer. *Proc. Natl Acad. Sci. USA*, **100**, 4539–4544.
25. Tanaka,K.J., Ogawa,K., Takagi,M., Imamoto,N., Matsumoto,K. and Tsujimoto,M. (2006) RAP55, a cytoplasmic mRNP component, represses translation in Xenopus oocytes. *J. Biol. Chem.*, **281**, 40096–40106.
26. Mili,D., Georgesse,D. and Kenani,A. (2015) Localization and role of RAP55/LSM14 in HeLa cells: a new finding on the mitotic spindle assembly. *Acta Biochim. Pol.*, **62**, 613–619.
27. Zhang,T., Li,Y., Li,H., Ma,X.S., Ouyang,Y.C., Hou,Y., Schatten,H. and Sun,Q.Y. (2017) RNA-associated protein LSM family member 14 controls oocyte meiotic maturation through regulating mRNA pools. *J. Reprod. Dev.*, **63**, 383–388.
28. Winata,C.L. and Korzh,V. (2018) The translational regulation of maternal mRNAs in time and space. *FEBS Lett.*, **592**, 3007–3023.
29. Dobretsov,M., Petkau,G., Hayar,A. and Petkau,E. (2017) Clock scan protocol for image analysis: imageJ plugins. *J. Vis. Exp.*,(124), 55819.
30. Dalton,C.M. and Carroll,J. (2013) Biased inheritance of mitochondria during asymmetric cell division in the mouse oocyte. *J. Cell Sci.*, **126**, 2955–2964.
31. Kamerkar,S.C., Kraus,F., Sharpe,A.J., Pucadyil,T.J. and Ryan,M.T. (2018) Dynamin-related protein 1 has membrane constricting and severing abilities sufficient for mitochondrial and peroxisomal fission. *Nat. Commun.*, **9**, 5239.
32. Adhikari,D., Lee,I.W., Al-Zubaidi,U., Liu,J., Zhang,Q.H., Yuen,W.S., He,L., Winstanley,Y., Sesaki,H., Mann,J.R., *et al.* (2022) Depletion of oocyte dynamin-related protein 1 shows maternal-effect abnormalities in embryonic development. *Sci. Adv.*, **8**, eabl8070.
33. Prasad,S., Tiwari,M., Pandey,A.N., Shrivastav,T.G. and Chaube,S.K. (2016) Impact of stress on oocyte quality and reproductive outcome. *J. Biomed. Sci.*, **23**, 36.
34. Aitken,R.J. (2020) Impact of oxidative stress on male and female germ cells: implications for fertility. *Reproduction*, **159**, R189–r201.
35. Sha,Q.Q., Zheng,W., Wu,Y.W., Li,S., Guo,L., Zhang,S., Lin,G., Ou,X.H. and Fan,H.Y. (2020) Dynamics and clinical relevance of maternal mRNA clearance during the oocyte-to-embryo transition in humans. *Nat. Commun.*, **11**, 4917.
36. Tanaka,T.S., Jaradat,S.A., Lim,M.K., Kargul,G.J., Wang,X., Grahovac,M.J., Pantano,S., Sano,Y., Piao,Y., Nagaraja,R., *et al.* (2000) Genome-wide expression profiling of mid-gestation placenta and embryo using a 15,000 mouse developmental cDNA microarray. *Proc. Natl Acad. Sci. USA*, **97**, 9127–9132.
37. Li,J., Qian,W.P. and Sun,Q.Y. (2019) Cyclins regulating oocyte meiotic cell cycle progression. *Biol. Reprod.*, **101**, 878–881.
38. Li,J., Ouyang,Y.C., Zhang,C.H., Qian,W.P. and Sun,Q.Y. (2019) The cyclin B2/CDK1 complex inhibits separase activity in mouse oocyte meiosis I. *Development*, **146**, dev182519.

39. Li,H., Zhao,H., Yang,C., Su,R., Long,M., Liu,J., Shi,L., Xue,Y. and Su,Y.Q. (2023) LSM14B is an oocyte-specific RNA-binding protein indispensable for maternal mRNA metabolism and oocyte development in mice. *Adv. Sci. (Weinh.)*, **10**, e2300043.
40. Rong,Y., Ji,S.Y., Zhu,Y.Z., Wu,Y.W., Shen,L. and Fan,H.Y. (2019) ZAR1 and ZAR2 are required for oocyte meiotic maturation by regulating the maternal transcriptome and mRNA translational activation. *Nucleic Acids Res.*, **47**, 11387–11402.
41. Ladomery,M. and Sommerville,J. (2015) The Scd6/Lsm14 protein xRAPB has properties different from RAP55 in selecting mRNA for early translation or intracellular distribution in Xenopus oocytes. *Biochim. Biophys. Acta*, **1849**, 1363–1373.
42. Flemr,M., Ma,J., Schultz,R.M. and Svoboda,P. (2010) P-body loss is concomitant with formation of a messenger RNA storage domain in mouse oocytes. *Biol. Reprod.*, **82**, 1008–1017.
43. Ernoult-Lange,M., Baconnais,S., Harper,M., Minshall,N., Souquere,S., Boudier,T., Bénard,M., Andrey,P., Pierron,G., Kress,M., *et al.* (2012) Multiple binding of repressed mRNAs by the P-body protein Rck/p54. *RNA*, **18**, 1702–1715.
44. Eulalio,A., Behm-Ansmant,I. and Izaurralde,E. (2007) P bodies: at the crossroads of post-transcriptional pathways. *Nat. Rev. Mol. Cell Biol.*, **8**, 9–22.
45. Yang,W.H., Yu,J.H., Gulick,T., Bloch,K.D. and Bloch,D.B. (2006) RNA-associated protein 55 (RAP55) localizes to mRNA processing bodies and stress granules. *RNA*, **12**, 547–554.
46. Hubstenberger,A., Courel,M., Bénard,M., Souquere,S., Ernoult-Lange,M., Chouaib,R., Yi,Z., Morlot,J.B., Munier,A., Fradet,M., *et al.* (2017) P-body purification reveals the condensation of repressed mRNA regulons. *Mol. Cell*, **68**, 144–157.

Received: May 5, 2023. **Revised:** October 1, 2023. **Editorial Decision:** October 3, 2023. **Accepted:** October 9, 2023